BRAIN
ORIGINAL ARTICLE

Onset pattern of nigrostriatal denervation in early Parkinson's disease

José A. Pineda-Pardo,[1,2,3,†] Álvaro Sánchez-Ferro,[1,4,†] Mariana H. G. Monje,[1,2,3,5] Nicola Pavese[6,7] and José A. Obeso[1,2,3]

[†]These authors contributed equally to this work.

The striatal dopaminergic deficit in Parkinson's disease exhibits a typical pattern, extending from the caudal and dorsal putamen at onset to its more rostral region as the disease progresses. Clinically, upper-limb onset of cardinal motor features is the rule. Thus, according to current understanding of striatal somatotopy (i.e. the lower limb is dorsal to the upper limb) the assumed pattern of early dorsal striatal dopaminergic denervation in Parkinson's disease does not fit with an upper-limb onset. We have examined the topography of putaminal denervation in a cohort of 23 recently diagnosed *de novo* Parkinson's disease patients and 19 age-/gender-matched healthy subjects assessed clinically and by ^{18}F-DOPA PET; 15 patients were re-assessed after 2 years. There was a net upper-limb predominance of motor features at onset. Caudal denervation of the putamen was confirmed in both the more- and less-affected hemispheres and corresponding hemibodies. Spatial covariance analysis of the most affected hemisphere revealed a pattern of ^{18}F-DOPA uptake rate deficit that suggested focal dopamine loss starting in the posterolateral and intermediate putamen. Functional MRI group-activation maps during a self-paced motor task were used to represent the somatotopy of the putamen and were then used to characterize the decline in ^{18}F-DOPA uptake rate in the upper- and lower-limb territories. This showed a predominant decrement in both hemispheres, which correlated significantly with severity of bradykinesia. A more detailed spatial analysis revealed a dorsoventral linear gradient of ^{18}F-DOPA uptake rate in Parkinson's disease patients, with the highest putamen denervation in the caudal intermediate subregion (dorsoventral plane) compared to healthy subjects. The latter area coincides with the functional representation of the upper limb. Clinical motor assessment at 2-year follow-up showed modest worsening of parkinsonism in the primarily affected side and more noticeable increases in the upper limb in the less-affected side. Concomitantly, ^{18}F-DOPA uptake rate in the less-affected putamen mimicked that recognized on the most-affected side. Our findings suggest that early dopaminergic denervation in Parkinson's disease follows a somatotopically related pattern, starting with the upper-limb representation in the putamen and progressing over a 2-year period in the less-affected hemisphere. These changes correlate well with the clinical presentation and evolution of motor features. Recognition of a precise somatotopic onset of nigrostriatal denervation may help to better understand the onset and progression of dopaminergic neurodegeneration in Parkinson's disease and eventually monitor the impact of putative therapies.

1 HM CINAC (Centro Integral de Neurociencias Abarca Campal), Hospital Universitario HM Puerta del Sur, HM Hospitales, Madrid, Spain
2 Universidad San Pablo-CEU, Madrid, Spain
3 CIBERNED, Instituto de Salud Carlos III, Madrid, Spain
4 Neurology Department, Hospital Universitario 12 de Octubre, Madrid, Spain
5 Ken and Ruth Davee Department of Neurology, Northwestern University, Feinberg School of Medicine, Chicago, IL, USA
6 Department of Nuclear Medicine and PET Centre, Aarhus University Hospital, Aarhus, Denmark
7 Translational and Clinical Research Institute, Newcastle University, Newcastle upon Tyne, UK

Received April 07, 2021. Revised September 06, 2021. Accepted September 09, 2021. Advance access publication March 29, 2022

Correspondence to: Jose A. Obeso
CINAC HM Puerta del Sur University Hospital, Móstoles, Madrid 28939, Spain
E-mail: jobeso.hmcinac@hmhospitales.com

Keywords: Parkinson's disease; ^{18}F-DOPA; dopamine; somatotopy; nigrostriatal system

Abbreviations: HS = healthy subject; LAS = less-affected side; MAS = more-affected side; UPDRS = Unified Parkinson's Disease Rating Scale

Introduction

Dopaminergic striatal denervation caused by progressive degeneration of dopaminergic neurons in the substantia nigra pars compacta (SNpc) is, along with Lewy body inclusions, the major pathological hallmark of Parkinson's disease. Clinically, this is linked to cardinal motor features of Parkinson's disease. Early in the evolution of Parkinson's disease, neurodegeneration is known to affect mainly the ventrolateral SNpc[1,2] and its projection to the posterolateral putamen, leading to prominent caudal dopaminergic denervation as demonstrated *in vivo* by presynaptic dopaminergic imaging using PET.[3,4] When the disease progresses, the dopaminergic deficit extends beyond the motor striatal territory to the more rostral associative putamen and the head of the caudate nucleus[5–10] and to other extrastriatal regions.[11,12] Minimal attention has been paid to the topography of denervation along the dorsoventral axis of the striatum, which could indicate a focal pattern of onset of degeneration.[4,13]

The somatotopic representation of the caudal motor putamen has been well defined in macaques by anatomy and physiological methods[14,15] and in humans with functional MRI.[16] Such somatotopic representation follows a dorsoventral direction with the lower limb dorsal, the upper limb at the intermediate level and the face ventrally placed. Two prior PET studies in Parkinson's disease suggested predominant dorsal dopaminergic denervation.[4,8] Accordingly, the anatomic–functional somatotopy of the motor putamen would predict that the earliest motor signs would generally be identified in the lower limbs.[17] Whereas general clinical experience suggests that the upper limb is most often affected at the time of diagnosis, an unequivocal clinical onset pattern has not been reported until now. Whether there is a net correlation between the clinical somatotopic onset of motor features and *in vivo* dopaminergic loss is not known.

We used 6-[^{18}F]-fluoro-L-dopa (^{18}F-DOPA) PET imaging in a cohort studied in detail comprised of both recently diagnosed *de novo* Parkinson's disease patients who were followed for 2 years and a group of healthy subjects (HS).[18] We analysed the striatal dopaminergic topography in both groups using voxel-wise, spatial covariance[19] and slice-wise analyses. Furthermore, the somatotopy of the putamen was defined using publicly available functional motor activation maps from the Human Connectome Project (HCP) dataset,[20] and ^{18}F-DOPA was quantified in the putamen as a weighted-average by the strength of the activation maps representing the upper and lower limb functional territories. In this cohort, we found a net predominant upper limb clinical onset.[18] In this report, we detail how these clinical findings correspond quite closely to predominant reduction of ^{18}F-DOPA uptake rate of the contralateral upper limb representation in the motor putamen. Furthermore, the putamina exhibited a similar progression pattern with different time of onset and evolution.

Materials and methods

Participants

Forty-three participants were included in this study (23 *de novo* Parkinson's disease and 20 gender- and aged-matched HS). Subjects were recruited consecutively and studied (baseline assessment) from December 2015 until July 2018. Inclusion criteria were: *de novo* patients diagnosed according to the UK Brain Bank Clinical Criteria who presented with unilateral cardinal motor features <18 months since diagnosis, as previously described.[18] Neurological exams included the Movement Disorders Society Unified Parkinson's Disease Rating Scale (MDS-UPDRS), Non-Motor Symptoms questionnaire (NMSQ) and the Parkinson's Disease Questionnaire (PDQ-39). Patients were drug-naïve at the time of study. MDS-UPDRS-III subscores of upper and lower limbs were calculated for each side to allow a direct comparison between upper and lower limbs. The upper limb subscore included rest tremor, rigidity, finger taps and pronation–supination movements of the hand (range 0–16); and the lower limb subscore included rest tremor, rigidity, toe-tapping and leg agility (range 0–16). Hand-grasp scores were not included to facilitate direct comparison between limbs, i.e. keeping four items in each subscore. Upper and lower limb subscores were also added together to evaluate clinical asymmetry between hemibodies (range 0–32). Objective quantitative metrics of MDS-UPDRS-III bradykinesia tasks were also studied kinematically using inertial measurement units (IMUs; Kinesia™ One system; Great Lakes Neurotechnologies Inc., Cleveland, OH)[21] as previously described.[18] Briefly, for the quantitative motor function evaluation, an IMU was placed on the index finger for upper limb tasks and on the heel of the shoe for lower limb tasks. Output data from Kinesia™ are a continuous score from 0 (none) to 4 (maximum) impairment.

The study protocol was approved by the Ethics Committee of HM Hospitales (protocol number: 16.10.0993-GHM) and written informed consent was obtained from all participants. One healthy control was excluded due to an artefact related to reconstruction of the PET images. Thus, 19 HS and 23 *de novo* Parkinson's disease patients were included in the final analysis. The two groups were comparable in terms of age, gender and handedness ($P > 0.05$; Table 1). Parkinson's disease patients were re-studied around 2 years after the initial visit in the period from February 2019 to February 2020. Eight Parkinson's disease patients did not complete the 2-year visit, mainly due to restrictions related to the current COVID-19 epidemic. The follow-up group included 15 subjects. The upper limb was clinically and kinematically the predominantly affected site of onset in 20 (87%) patients and the right body side

was the most affected side in 15 (65%). In 12 Parkinson's disease patients (52%) there were no evident motor signs on the less-affected side, i.e. the MDS-UPDRS III was 0. At the 2-year follow-up three (13%) patients still had no motor signs on the less-affected side.

Image acquisition and preprocessing

PET imaging was performed on a hybrid 3T mMR-Biograph system (Siemens Healthcare) at baseline (HS, PD_{BL}) and at 2 years (PD_{2y}). Images were acquired in the morning, at rest and after 6 h of fasting. None of the patients had received any anti-parkinsonian drugs before the first ^{18}F-DOPA PET scan. By the time of the second visit, all subjects had been placed on dopaminergic medication: 10 received pramipexol 1.05–2.1 mg/day or rotigotine patch (8 mg/day); 13 received rasagiline (1 mg daily); and 5 were on levodopa (190 mg/day), which were interrupted at least 48 h before the study. Carbidopa (50 and 200 mg p.o.) was administered orally 12 h and 1 h before the PET exam. All subjects were studied in the supine position. PET acquisition started immediately following intravenous injection of ~5 mCi of ^{18}F-DOPA (average dose 5.15 ± 0.22 mCi). PET data were acquired during 90 min in list-mode. PET emission data were reconstructed with an ordered subset-expectation maximization algorithm, smoothed using a 4-mm full-width half-maximum 3D Gaussian kernel and corrected for attenuation using four-compartment MR-based maps derived from a dual-echo Dixon-based sequence (repetition time = 3.6 ms, echo time = 1.23–2.46 ms) that also incorporates bone information using a model-based segmentation algorithm.[22] Twenty-two time frames of PET activity were reconstructed: 90 s (10 frames), 300 s (nine frames) and 600 s (three frames). Reconstructed images had a matrix size of 344 × 344 × 127 and a voxel size of 2.09 × 2.09 × 2.03 mm^3.

Simultaneous with the PET acquisition, several MRI sequences were acquired: 3D T_1-weighted magnetization-prepared rapid acquisition gradient-echo (176 sagittal slices; TR/TE/TI = 2300/3.34/900 ms; flip angle = 8°; slice thickness = 1 mm; acquisition matrix = 256 × 256; FOV = 256 × 256 mm^2) and 3D T_2-weighted turbo spin-echo (176 sagittal slices; TR/TE = 3200/418 ms; flip angle = 120°; slice thickness = 1 mm; acquisition matrix = 256 × 256; FOV = 256 × 256 mm^2). The scans (both PET and MRI) of the patients who had more prominent left hemibody motor signs (n = 8) were flipped over, so that the left hemisphere images represented the more-affected side (MAS), while the less-affected side (LAS) corresponded to the right hemisphere. HS group images were also flipped along the left–right axis according to hand dominance, i.e. left hemisphere would correspond to the dominant side and right hemisphere would correspond to the non-dominant side.

Image pre-processing was performed using the FMRIB Software Library v6.0 (FSL; https://fsl.fmrib.ox.ac.uk/fsl/fslwiki/; accessed 7 February 2022) and Advance Normalization Tools (ANTs; http://stnava.github.io/ANTs/; accessed 7 February 2022)[23] software libraries and in-house scripts developed in MATLAB (MathWorks Inc., USA, R2018b). T_1-weighted MRI images were corrected for intensity bias using an N4 bias correction algorithm[24] denoised using an optimized non-local means filter[25] and skull-stripped using a brain extraction tool (BET-FSL).[26] The putamen region was automatically segmented on denoised T_1-weighted images using the FMRIB Integrated Registration and Segmentation Tool (FIRST-FSL).[27] Skull-stripped images were normalized into the Montreal Neurological Institute standard space (MNI space), using the symmetric T_1-weighted MNI template with 1 mm isotropic resolution (MNI152 NLIN2009) as reference.[28] An affine transformation was followed by the symmetric image normalization algorithm (SyN) in ANTs.[23] PET image frames were spatially co-registered within subjects with a rigid body transformation to reduce the effects of subject motion during the imaging session using the intramodal motion correction FMRIB Linear Image Registration Tool (MCFLIRT-FSL).[29] Voxel-based ^{18}F-DOPA uptake rate (expressed as influx constant K_i [min^{-1}]) maps were estimated using the Patlak graphical method[30] and taking the average time activity curve from an occipital lobe mask as reference. Uptake rates were scaled by 1000 for representation [1000 · min^{-1}]. Follow-up T_1-weighted images were rigidly realigned to baseline acquisitions. Finally, ^{18}F-DOPA K_i maps, both baseline and 2-year longitudinal follow-up, were normalized into MNI space by reapplying the same transformations as estimated for the T_1-weighted images.

Table 1 Demographic characteristics and clinical features of Parkinson's disease patients

	HS (n = 19)	Parkinson's disease (n = 23)	P-value (Parkinson's disease versus HS)
Baseline demographic characteristics			
Age	49.0 [45.1–61.9]	56.7 [48.4–63.1]	0.15
Gender (male/female)	(9/10)	(13/10)	0.78
Handedness (right/left)	(17/2)	(18/3)	1
Parkinson's disease patient characteristics at baseline			
Time since diagnosis (months)		6.1 [2.8–8.1]	
Time from onset (months)		8.3 [6.1–13.5]	
Side of onset (right/left)		(15/8)	

Clinical evaluation	Baseline (n = 23)	2 years (n = 15)
MDS-UPDRS III	16.0 [13.0–26.0]	24.0 [18.0–29.5]
MAS—MDS-UPDRS III (/32)	9.0 [6.5–11.0]	10.0 [9.0–13.5]
MAS—Upper-limb subscore (/16)	5.0 [5.0–6.5]	6.0 [5.0–7.5]
MAS—Lower-limb subscore (/16)	3.0 [2.0–5.0]	4.0 [4.0–5.0]
LAS—MDS-UPDRS III (/32)	0.0 [0.0–2.5]	3.0 [1.0–4.0]
LAS—Upper-limb subscore (/16)	0.0 [0.0–2.0]	2.0 [1.0–2.5]
LAS—Lower-limb subscore (/16)	0.0 [0.0–1.0]	1.0 [0.0–1.5]

Continuous variables are reported as medians and interquartile ranges. Categorical variables are reported as counts. Statistical comparisons between Parkinson's disease and HS groups were performed with the Mann–Whitney U-test non-parametric test for age and with the chi-square test for categorical variables. MDS-UDRS subscores were computed as the sum of rest tremor, rigidity, finger taps and pronation–supination movement items for the upper limb; and as the sum of rest tremor, rigidity, toe-tapping and leg agility items for the lower limbs (each subscore with a maximum of 16 points). Axial scores were not included in the lateralized (more- or less-affected sides) MDS-UPDRS.

Image analysis

Image analysis was performed using Statistical Parametric Mapping software (SPM12; https://www.fil.ion.ucl.ac.uk/spm/software/spm12/; accessed 7 February 2022) for voxel-based comparison and in-house scripts developed in MATLAB (MathWorks Inc., USA, R2018b). Whole-brain voxel-based comparison of normalized K_i maps between HS and PD_{BL} groups was carried out using a univariate two-sample *t*-test comparison. The Cohen's *d* effect size striatal voxel-based maps were estimated between HS and PD_{BL}, and between HS and PD_{2y} groups.

Spatial covariance analysis was done to extract group-specific striatal components that may account for Parkinson's disease differential diagnosis or clinical severity.[19] ^{18}F-DOPA K_i maps from HS and PD_{BL} groups were masked at the striatum using a predefined basal ganglia atlas,[31] then striatal voxels for all subjects were reordered in a matrix of 42 subjects (rows) by the number of voxels (columns). Row averages were subtracted to represent subject-wise deviations from average, and subsequently column averages were subtracted to create the subject residual profile. Principal component analysis was applied to the covariance matrix to identify the spatial covariance patterns. Subject expression values of the spatial patterns were then extracted for PD_{BL} and PD_{2y} subjects and standardized (Z-score) to the HS group.

Region of- interest analyses followed two approaches: (i) a slice-wise analysis taking the average K_i across axial sliced sections of the post-commissural putamen[32]; and (ii) a region-wise analysis using a functional parcellation of the putamen based on functional MRI motor activations. For the latter a somatotopic map of the putamen was defined by functional MRI group activation maps from a motor task performed by 889 normal subjects (WU-Minn HCP 1200 Subjects Data Release).[20,33] The motor task consisted of a block design where participants were asked to perform a series of movements—finger tapping, toe squeezing, or tongue movements—when a visual cue was presented. Further details of the collection, pre-processing and analysis of the data can be found elsewhere.[34] Somatotopic Cohen's *d* effect-size maps for hand and foot motor activations were masked to the putamen contralateral to the movement using a subject-specific segmentation. Then, K_i values were linearly weighted by Cohen's *d* effect sizes and averaged for all voxels within the putamen. In a secondary analysis the same weighted averages were obtained but restricted to the contralateral post-commissural putamen. The face functional representation was not included as part of the somatotopic parcellation, because spontaneous facial movements are bilateral and recruit both hemispheres. Furthermore, we lack an accurate clinical evaluation of facial expression/movements and the current scale of hypomimia provides poor sensitivity.

While all analyses presented here were performed without correcting for partial volume errors (PVE), for completeness, a slice-wise analysis was repeated after adding the PVE correction to ^{18}F-DOPA PET images with the voxel-based modified Müller–Gärtner method available in the PVE-Lab software package.[35]

Statistics

Comparison of demographic characteristics between Parkinson's disease patients and HS were performed using non-parametric Mann–Whitney U-tests for continuous variables and chi-square tests for categorical variables. Statistical significance in the voxel-based comparison was established for a family-wise error (FWE) corrected P-value lower than 0.05 at the voxel level. Subject pattern expression scores and K_i average values were compared between groups (PD_{BL}/PD_{2y}/HS) using non-parametric Mann–Whitney U-tests, separately for the MAS (dominant side in HS) and LAS (non-dominant side in HS).

Percentage changes in K_i values were estimated between groups (Parkinson's disease versus HS and PD_{2y} versus HS). K_i values were standardized (Z-score), and the Wilcoxon signed-rank test was performed to facilitate within-subject comparison between upper- and lower-limb K_i loss in the PD_{BL} and PD_{2y} groups. Two-way repeated-measures ANOVA was performed to identify significant interaction effects between visits (baseline, 2 years), region of interest (upper limb, lower limb) and between visits and brain side (MAS, LAS). In a *post hoc* analysis, decline in striatal K_i across visits was quantified as the paired gross change between Z-score standardized values. Using a Wilcoxon signed-rank test we compared pair-wise differences in progression between regions of interest and between sides.

Non-parametric correlation analysis (Spearman correlations) was performed between imaging (K_i values) and clinical measures (Kinesia aggregate scores for upper or lower limbs). From the region of interest analyses, 12 correlations were tested, eight of them between the K_i of each functional putaminal functional subdivision and the kinematic evaluation of the corresponding limb, in both PD_{BL} and PD_{2y} groups, and four additional correlations testing the association between decline in K_i and percent change in kinematic metrics across visits. From the spatial covariance analysis, the same correlations were tested between the expression values from each relevant spatial pattern and the kinematic metrics. In two Parkinson's disease patients, kinematic measurements could not be reliably obtained, and these were not included in the correlation analyses. The significance level was set at $P < 0.05$, and R version 1.1.463 was used for all data management and statistical analysis.

Data availability

The data that support the findings of this study are available upon reasonable request.

Results

The median disease duration for the patients was 6.1 (IQR 2.8–8.1) months, and the median MDS-UPDRS-III score was 16 (IQR 13–26) points, highly confined to one hemibody (Table 1). ^{18}F-DOPA K_i maps showed a net inter-hemispheric asymmetry and a rostrocaudal gradient with greater reduction in the caudal putamen (Fig. 1) in all 23 Parkinson's disease patients at baseline. Voxel-based comparison of the K_i images between the Parkinson's disease and HS groups revealed two significant clusters of K_i reduction in either caudal putamen of the Parkinson's disease group at baseline (FWE-corrected $P < 0.05$ at the voxel level; Fig. 2A).

The somatotopic functional specificity of these clusters was tested using functional regions of interest corresponding to the hand and foot activation subregions from the task-functional MRI

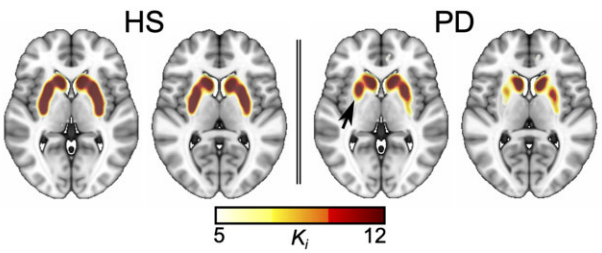

Figure 1 Representative K_i map for a healthy subject and a *de novo* Parkinson's disease patient. Characteristically predominant reduction in ^{18}F-DOPA uptake rate in the caudal putamen contralateral to the most affected clinical side is highlighted with a black arrow.

HCP dataset. These activation maps were thresholded at Cohen's $d > 0.3$ and overlaid onto Cohen's d effect-size maps in the striatum (Fig. 2B). The area with the largest K_i reduction appears to cover the boundary between lower and upper limb functional territories in the putamen but extends further into the hand functional division (Fig. 2C). A similar but attenuated pattern, i.e. smaller difference between controls and patients, was present in the less-affected putamen. At 2 years, the pattern was stable on the MAS, while it showed clear progression on the LAS.

Spatial covariance analysis revealed a spatial pattern (first principal component) which stood out from the rest and accounted for 42.2% of the variance (Fig. 3A and B), with the second and third principal components showing an explained variance of 7.3% and 4.6%, respectively. The subject scores for the first pattern were a strong discriminator between HS and PD_{BL} patients ($P < 0.001$) (Fig. 3C). Furthermore, at 2 years a progression in expression of the pattern was observed ($P < 0.001$) (Fig. 3C). Expression values of the second and third components did not show discrimination capacity between groups and were not sensitive to progression; therefore, we did not consider them relevant for further analysis. Regarding topography, the first pattern confirmed a rostrocaudal and mediolateral intensity gradient that outlined the topography of ^{18}F-DOPA deficit (from less to more severe) that resembles the typical ^{18}F-DOPA PET pattern of an early Parkinson's disease patient (Fig. 1), including clear asymmetry between the more- and less-affected striatum. These findings confirm with a different approach that dopaminergic denervation of the caudal putamen, judged by ^{18}F-DOPA PET, follows a centripetal dorsoventral pattern centred in the mid-putamen subregion. This in turn corresponds to the somatotopic representation of the upper limb, coinciding and confirming the relationship between clinical findings and ^{18}F-DOPA PET. Importantly, this pattern is intensified at 2 years and also corresponds to the clinical progression. The caudate nucleus also showed a mediolateral intensity gradient and dorsal predominance of ^{18}F-DOPA uptake loss (Fig. 3B), but these changes were less noticeable and will require a larger number of subjects for adequate ascertainment.

^{18}F-DOPA K_i were averaged within the putamen weighted by the functional group activations (upper and lower limbs). Weighted-average K_i differed significantly between HS and Parkinson's disease patients at both time points, baseline and 2 years, for both regions and in both hemispheres ($P < 0.001$; Fig. 4A and Table 2). The median percentage reduction on the more-affected side was 58.4% for the foot subdivision and 63.6% for the hand subdivision. On the less-affected side, these percentages were 37.7% in the foot and 43.2% in the hand. Such differences between the lower- and upper-limb subregions were small but nevertheless significant, i.e. greater loss in the hand region than in the foot area for both MAS ($Z_{hand} = -7.54$, $Z_{foot} = -5.95$; $P < 0.001$) and LAS ($Z_{hand} = -4.24$, $Z_{foot} = -3.28$; $P < 0.001$; Fig. 4B and Table 2). At 2-year follow-up, ^{18}F-DOPA K_i was reduced by 8% to 14% in less- and more-affected sides, respectively (Table 2). Significant interaction effects between time and brain side were found for the upper-limb progression ($P = 0.0340$) and between time and striatal region of interest in the less-affected side ($P = 0.0100$; Supplementary Fig. 1). *Post hoc* analysis revealed that: (i) change in

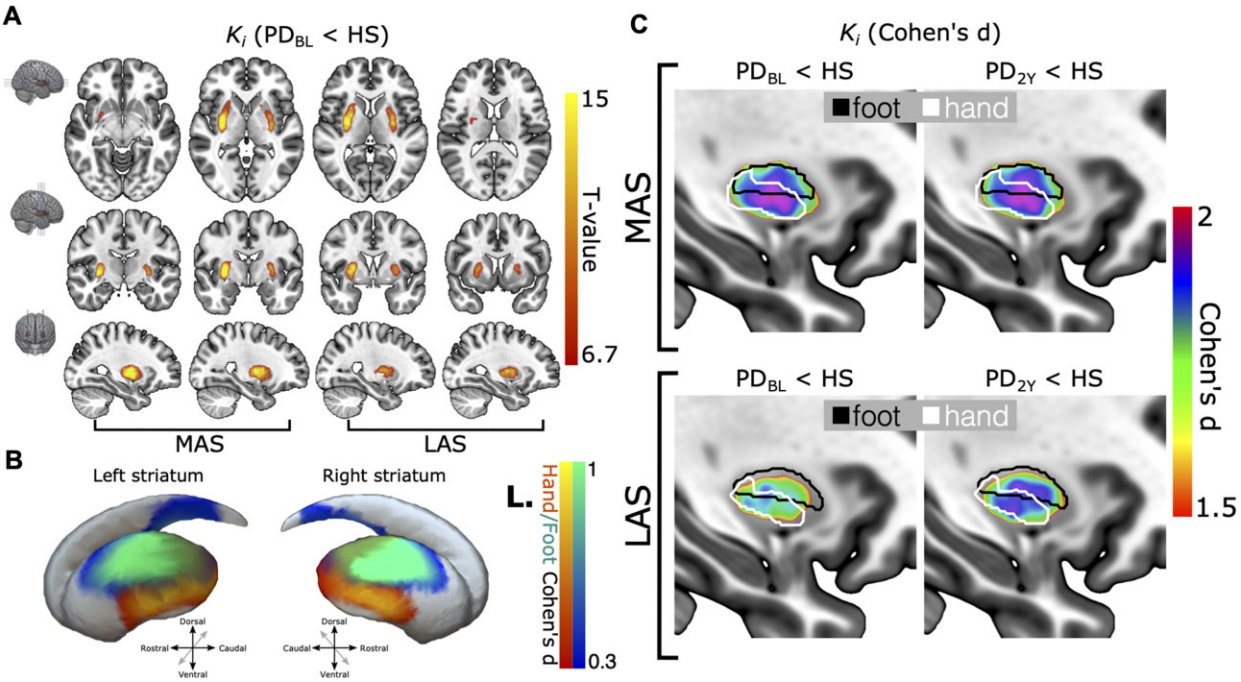

Figure 2 Voxel-based analysis. Voxel-based differences in striatal ^{18}F-DOPA uptake rate (K_i) representing the first and second study (2 years after first assessment). (**A**) Statistical map with $P < 0.05$ threshold (family-wise error correction for multiple comparisons at the voxel level) showing the reduction of K_i in the *de novo* Parkinson's disease group in a red–yellow colour map (more-affected/less-affected [MAS/LAS] sides). The map is overlaid onto an MNI space T_1-weighted template. (**B**) Lateral views of a striatal surface reconstruction with overlaid task-based functional MRI group activations associated with movements of the hand and foot. Activation maps are represented as Cohen's d effect sizes. Red–yellow and blue–green colour maps stand for hand and foot activations, respectively, and R./L. correspond to the right/left hemibody, i.e. left/right striatum. (**C**) Sagittal view of the Cohen's d effect size of differences between the striatal voxels between healthy subjects and Parkinson's disease patients at baseline and follow-up (2 years) study. Cohen's d maps are overlaid onto the MNI space T_1-weighted template. The contour of the functional territories for foot and hand activations (Cohen's $d > 0.3$), black and white, respectively, are also overlaid for the most-affected (*top*) and less-affected (*bottom*) sides. Altogether, these findings reveal a predominant K_i reduction in the caudal intermediate putamen, which mainly corresponds with the upper-limb representation.

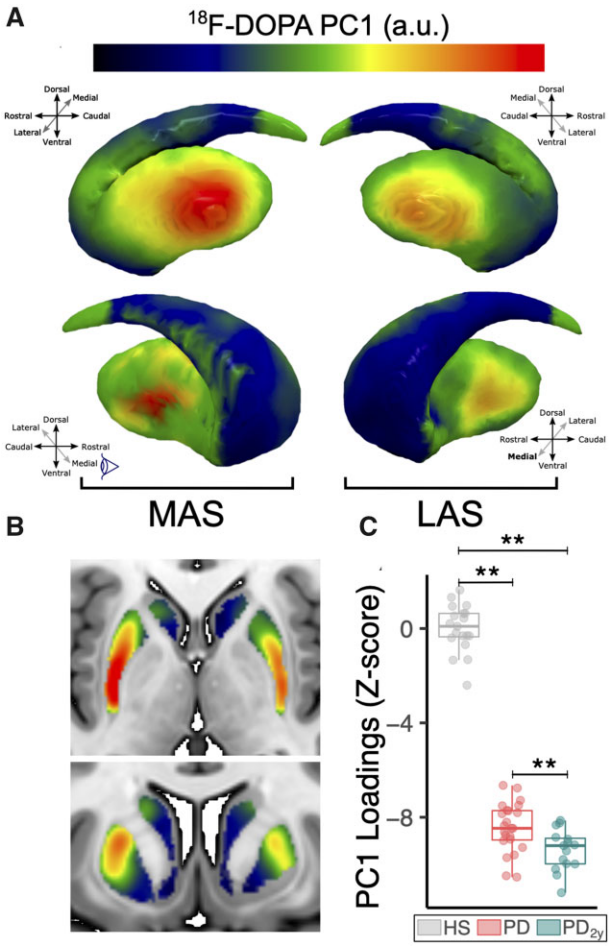

Figure 3 Spatial covariance analysis. (**A**) Representation of the extracted covariance pattern overlaid onto the striatal surface from lateral and medial angle views showing the focal onset of denervation in the posterolateral putamen in both the more-affected and less-affected sides. (**B**) Two-dimensional axial and coronal slices of the pattern overlaid onto the MNI space T_1-weighted template emphasizes the observed intensity gradients in rostrocaudal and mediolateral axes. (**C**) Box plot representation showing subject pattern expression values for the described bilateral striatum pattern, which shows significant discrimination between HS and Parkinson's disease groups and is sensitive to progression at 2 years (**$P < 0.001$ after non-parametric Mann–Whitney U-test). Box plot and individual values are represented in grey for HS, red for Parkinson's disease at baseline and green for Parkinson's disease at 2-year follow-up.

progression between visits in the upper limb was larger for the LAS than for the MAS ($P = 0.0302$); (ii) the upper limb progressed faster than the lower limb in the LAS ($P = 0.0151$); and (iii) there was a trend for the upper limb progressing faster than the lower limb in the more-affected side ($P = 0.0946$). Thus, progression of dopaminergic loss occurred mainly in the hand subregion bilaterally but particularly in the primarily less-affected hemisphere, which was also the side showing more significant motor worsening clinically.[18] Subsequently, the same weighted averages were obtained but restricted to the post-commissural putamen. This confirmed the greater loss of ^{18}F-DOPA K_i for the hand (Supplementary Fig. 3A and B) and, in addition we found that HS had a greater ^{18}F-DOPA K_i in the hand than in the foot division (Supplementary Table 1). This result was not present when taking the weighted average across the whole putamen.

The pattern of ^{18}F-DOPA K_i loss through the dorsoventral putaminal axis was further ascertained by slice-wise analysis of the average K_i (Fig. 4C and D). In the HS group K_i shows a non-linear distribution with maximum at the boundary between upper and lower limb putaminal subregions; in the Parkinson's disease group the K_i shows an overall reduction with a gradient whereby the dorsal sections of the putamen show the lowest ^{18}F-DOPA K_i at baseline and 2-year follow-up. However, Z-score normalization with HS control values revealed that the largest K_i loss on the MAS peaked at the centre of the hand functional subdivision (Fig. 4D). Thus, the impression of predominant dorsal dopaminergic depletion is not validated when proper spatial normalization is applied. On the LAS, it also seems to be more profound in the hand division, although the effect is less well-defined. This pattern persisted at 2 years for the MAS, whereas the LAS evolved towards similar ^{18}F-DOPA K_i values as shown in the MAS at baseline (Fig. 4C). Progression on the LAS, when normalized to normal subjects, trended in the same fashion as the MAS but did not reach exactly the same profile (Fig. 4D). These results were all preserved even after introducing a partial volume correction stage (Supplementary Fig. 2).

Finally, we analysed the correlation between hand and foot movements (evaluated by kinematic analysis) and ^{18}F-DOPA K_i considering both baseline and follow-up values and K_i decline between time points. Kinesia-derived data for this population at baseline and 2 years were published in detail previously.[18] At baseline, K_i in the hand functional division of the MAS had a moderate correlation with the more-affected upper limb aggregated Kinesia score ($r = –0.56$, $P = 0.0086$). At 2-year follow-up such correlation for the upper limb in the MAS persisted ($r = –0.60$, $P = 0.0340$), and a correlation between the hand subdivision of the LAS and the upper-limb Kinesia score showed statistical significance ($r = –0.72$, $P = 0.0075$). In addition, correlations between ^{18}F-DOPA K_i in the foot subdivision of the MAS and the lower-limb Kinesia score ($r = –0.49$, $P = 0.0889$) and between the foot subdivision of the LAS and the lower-limb Kinesia score ($r = –0.51$, $P = 0.0812$) showed a tendency towards statistical significance. Thus, assessment of bradykinesia with the aid of the Kinesia system allows us to further define a relationship between putaminal ^{18}F-DOPA K_i and movement impairment in the limbs. No correlations were found between worsening in the Kinesia scores and progression in ^{18}F-DOPA K_i, nor with the subject expression of the described spatial patterns.

Discussion

This study describes a specific topography of ^{18}F-DOPA uptake rate reduction within the nigrostriatal system in a selected population of a recently diagnosed drug-naive Parkinson's disease cohort. The main finding was a fairly localized maximum uptake rate loss in the rostrocaudal and dorsoventral axes of the caudal and intermediate putamen, respectively. The loss was located primarily on the most-affected side and corresponded mainly with the somatotopic representation of the upper limb. Importantly, it coincides with clinical onset in the upper limb, as previously described in this cohort.[18] The 2-year follow-up revealed a similar decline in the ^{18}F-DOPA uptake rate on the less-affected side that also corresponded to clinical motor worsening on that side. These results have several relevant implications.

Pattern of striatal DA denervation and clinical onset

^{18}F-DOPA K_i was reduced mainly in the caudal putamen as reported previously.[3–5,8] Significant decline in ^{18}F-DOPA K_i was overt in the putamen contralateral to the primarily affected side clinically, i.e. mostly the right upper limb, and less striking but also significant in the other hemisphere, contralateral to the less-affected body side. The caudal putamen corresponds to the motor

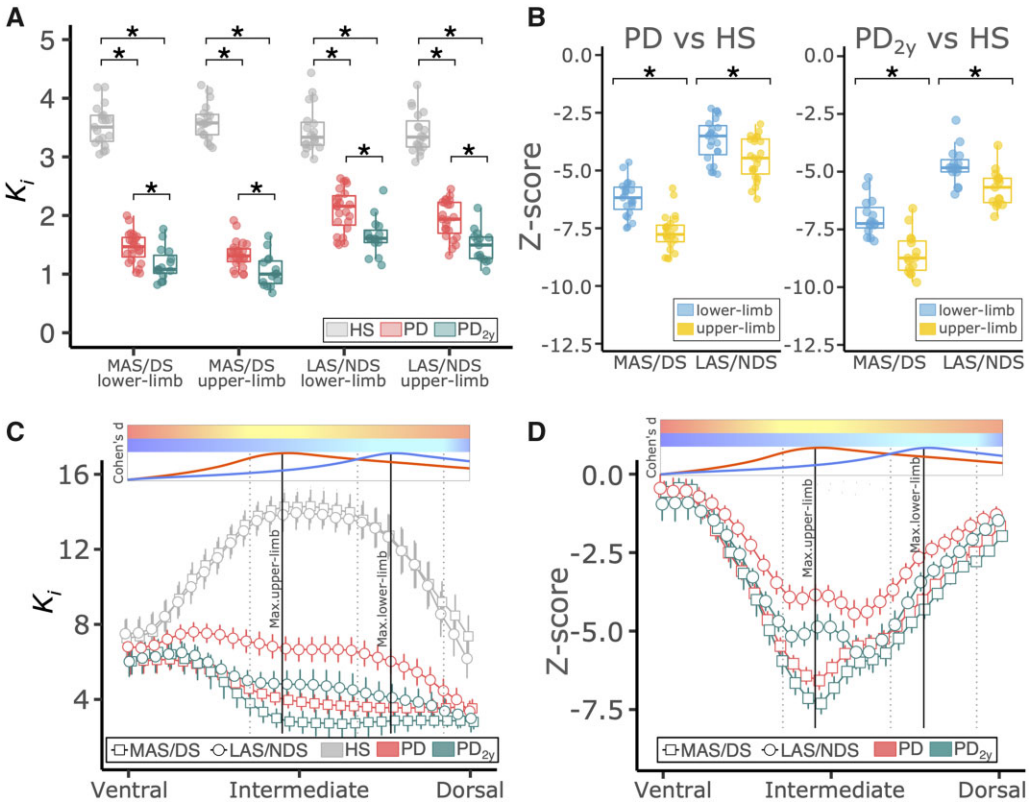

Figure 4 Region-based analysis of ^{18}F-DOPA uptake rates. (**A**) Box plots show weighted-average K_i values (median and perc$_{25\text{-}75}$) for HS (grey) and Parkinson's disease at baseline (red) and at 2-year follow-up (green). K_i values in the whole putamen contralateral the more-affected or less-affected side (MAS/LAS) were weighted by the strength (Cohen's *d*) of the upper- and lower-limb group activation functional MRI maps and averaged. *$P < 0.001$ with Mann–Whitney U-test. (**B**) Box plots show Z-scores for K_i weighted-average values (median and perc$_{25\text{-}75}$) normalized to HS for upper (yellow) and lower limb (light blue). *$P < 0.001$ with Wilcoxon signed-rank test. (**C**) Error bars show K_i slice-wise averages and confidence intervals (95%) in the post-commissural putamen from the most ventral to the most dorsal extent for HS (grey), Parkinson's disease at baseline (red) and at 2-year follow-up (green) on both the more-affected and less-affected sides. (**D**) Error bars show Z-scores (average and confidence interval) for K_i in Parkinson's disease normalized to HS, on the more-affected (squares) and less-affected (circles) sides. Parkinson's disease at baseline is represented in red and at 2-year follow-up in green. In **C** and **D** two colour bars represent the functional MRI normalized activation along the dorsoventral axis for the upper (red to yellow) and lower (dark blue to light blue) limbs. Below the colour bars two normalized curves show the strength of the group activation map along the dorsoventral axis. Maxima have been highlighted downwards with vertical lines. In dotted vertical lines the interval between the 75% of the maximum activation are also highlighted.

Table 2 ^{18}F-DOPA uptake rates for putaminal functional hand and foot subdivisions

Group	Region of interest	K_i (Parkinson's disease versus HS, %)	K_i (Parkinson's disease versus HS, Z)	K_i decline (%)	K_i decline (Z)
PD_{BL}	MAS—Foot	58.4 [53.9–63.3]	5.95 [5.50–6.46]	NA	NA
	MAS—Hand	63.6 [60.2–66.3]	7.54 [7.14–7.86]	NA	NA
	LAS—Foot	37.7 [32.6–47.0]	3.28 [2.83–4.09]	NA	NA
	LAS—Hand	43.2 [34.8–50.3]	4.24 [3.41–4.93]	NA	NA
PD_{2y}	MAS—Foot	69.4 [62.6–71.2]	7.07 [6.38–7.83]	8.2 [6.2–10.5]	0.84 [0.63–1.07]
	MAS—Hand	72.2 [76.7–66.0]	8.57 [7.83–9.09]	9.2 [5.2–12.3]	1.09 [0.61–1.46]
	LAS—Foot	53.5 [49.5–55.6]	4.66 [4.31–4.84]	14.4 [7.4–16.6]	1.26 [0.65–1.44]
	LAS—Hand	56.2 [52.2–62.9]	5.50 [5.11–6.16]	13.3 [10.1–16.7]	1.31 [0.99–1.64]

Differences in ^{18}F-DOPA K_i between Parkinson's disease patients and healthy subjects are assessed by percentage change and Z-score normalization. Decline in ^{18}F-DOPA K_i at 2-year follow-up was assessed in terms of percentage or gross Z-score differences. Reported values are presented as median [interquartile range].

domain within the functional striatal subdivisions.[14,36] Accordingly, these results fit well and further support a direct relationship between a certain degree of putaminal DA denervation and the onset of cardinal features in Parkinson's disease. Our data indicate that the threshold for detecting motor signs is around 60% of putaminal DA denervation, which coincides remarkably with what is found experimentally in non-human primates.[37] This estimate is fairly accurate, with due limitations, when considering the findings on the primarily less-affected side, which becomes symptomatic over 2 years. Patients had been evaluated periodically since the beginning of the study, and in most instances the second ^{18}F-DOPA PET was carried out close

to recognition (within less than a year) of parkinsonism on the LAS.

Earlier studies suggested a dorsoventral gradient of striatal dopaminergic denervation with a greater loss in the dorsolateral tier,[4,8,38] and a clinical study[17] based on the onset of levodopa-induced dyskinesias also proposed that a dorsoventral gradient of DA striatal denervation would best explain Parkinson's disease focal motor onset in the lower limbs. On the other hand, several authors reported upper-limb predominance at onset of Parkinson's disease.[39–43] We encountered a net upper-limb onset in patients' symptoms, neurological examination and a refined assessment including objective kinematic evaluation. Moreover, such upper-limb preponderance was also demonstrated in the independent Parkinson's Progression Markers Initiative (PPMI) cohort when we evaluated patients with very similar clinical characteristics.[18]

Our detailed analysis shows that dopaminergic denervation peaks in the intermediate sub-region of the caudal putamen and progressively extends bidirectionally in dorsal and ventral directions (Fig. 4D). This result appears, in principle, contrary to what Morrish *et al.*[4] concluded in their cross-sectional study by reporting a linear dorsoventral gradient of ^{18}F-DOPA K_i loss in Parkinson's disease patients who had longer disease duration than our cohort. Importantly, Morrish *et al.*[4] a used a single reference uptake by taking the average value in the healthy putamen, a method that would just reproduce the distribution of dopaminergic that we saw in Fig. 4C. However, we found that normal ^{18}F-DOPA K_i distribution is not constant but peaks precisely in the intermediate putaminal region, and therefore, when dorsoventral uptake distribution is assessed in Parkinson's disease versus HS, greater decline in ^{18}F-DOPA K_i arises in the middle–intermediate subregion of the human motor striatum. This analysis essentially resolves the issue of striatal dopaminergic denervation pattern in Parkinson's disease and provides a close correlation between the somatotopy of the motor putamen[16,44,45] and the predominant clinical onset in the upper limb.[18] We also found a moderate correlation between bradykinesia as measured by quantitative inertial sensors and the ^{18}F-DOPA decline.

These results are strongly corroborated by the findings at 2-year follow-up, particularly when assessing the less affected side. Thus, the topography of the ^{18}F-DOPA pattern of uptake rate loss encountered for the MAS at baseline was essentially found at 2 years for the LAS (Fig. 4D) and coincides with the development of motor signs in the upper limb of that side. This will be discussed in greater detail below.

Limitations

The main clinical limitations of the findings reported here are the relatively small number of patients enrolled in the study and the feasibility of ^{18}F-DOPA PET as a precise marker of nigrostriatal neurodegeneration. However, the group of patients recruited for the study represent a cohort of carefully ascertained early Parkinson's disease patients with predominant motor manifestations and focal presentation. These are all important strengths of the study, i.e. to recognize the onset pattern of nigrostriatal neurodegeneration and its clinical counterpart, and better defined than several other previous PET studies. Furthermore, the 2-year follow-up provided quite distinct and highly supportive information about the pattern of nigrostriatal loss discussed here.

We acquired ^{18}F-DOPA PET to account for striatal dopaminergic integrity indirectly through quantification of aromatic L-amino acid decarboxylase activity and dopamine storage capacity in nigrostriatal terminals. Admittedly, in an ideal scenario we could have used a vesicular monoamine transporter type 2 (VMAT2) PET tracer, which has been defined as more sensitive to striatal dopaminergic denervation.[46] Indeed, it has been proposed that ^{18}F-DOPA activity might be upregulated in early Parkinson's disease[46,47] and lead to lower sensitivity for early dopaminergic denervation. Even if this is the case, we believe that the findings are representative of this early evolutionary stage of Parkinson's disease, given the well-defined rostrocaudal pattern of K_i and the inter-hemispheric asymmetry. Multi-tracer studies have shown high correlation between ^{18}F-DOPA and VMAT2 uptakes in both cross-sectional[47,48] and longitudinal studies.[6] Furthermore, the reduction in ^{18}F-DOPA K_i fit well with quantitative estimations of hand and foot movements using an inertial system (Kinesia), thus establishing significant correlation between the striatal deficit evaluated by PET and motor behaviour. This supports the validity of ^{18}F-DOPA measurements for the evaluation carried out here. Admittedly, we did not ascertain facial movements or the facial putaminal somatotopic representation needed to complete the pattern of progression. Currently, we lack an accurate clinical scale to evaluate the asymmetry of facial activation in Parkinson's disease, and the bilateral corticostriatal representation of spontaneous facial movements needs to be taken into account. These aspects should be developed further.

Another relevant aspect is whether striatal somatotopy could be determined with the spatial specificity of standard PET acquisitions and the validity of the currently used somatotopic map. Thus, the limited spatial resolution, partial volume contamination and lack of anatomical detail in the PET images could hinder the capacity to differentiate these somatotopically arranged subregions. In this study, we used a hybrid PET-MR system, which has an average spatial resolution of 4.3 mm full width at half maximum.[49] During all PET exams, several MRI sequences were acquired, including a high-resolution structural T_1-weighted MRI, thus eliminating the need for inter-modal spatial co-registration and therefore improving the inter-subject comparison accuracy and compensating for the inherent limitations of PET. Moreover, we took advantage of such PET-MRI multimodal acquisition, and although the need for partial volume error correction is not standard in dopaminergic PET striatal quantification, we replicated our main results after introducing this correction stage (Supplementary Fig. 2).

The overlap observed between upper- and lower-limb putaminal divisions is also a matter of consideration. Spatial limitations in image resolution and processing might be relevant on this regard but this is unlikely considering the high quality in terms of both acquisition and processing of the HCP.[20] Such functional MRI functional overlap has been previously recognized[16] and importantly, it is well-described in monkeys by anatomical tracing studies.[14,15] It is also relevant to consider whether the somatotopic map, as recognized in macaques[45] and in humans with functional MRI,[16,44] could be valid in a study of a chronically evolving disorder associated with several compensatory mechanisms. Whereas direct data regarding the impact of striatal dopaminergic denervation on the homunculus representation are not available, distortions at the cortical and putamen level are possible. Neuronal recordings in the 1-methyl-4-phenyl-1,2,3,6-tetrahydropyridine (MPTP) monkey model and in Parkinson's disease patients in basal ganglia output nuclei have shown augmented responsiveness and receptive fields,[50] but have not revealed major changes in the anatomical representation of the body.[15,51–54] Accordingly, we would expect that the focal reduction in ^{18}F-DOPA uptake rate in the upper-limb region of the putamen represents a somatotopic-related finding.

Implications for pathogenesis

Focal onset

The reported focal onset of dopaminergic denervation in the caudal and intermediate subregion of the putamen and its strong

correspondence with the functional subdivision of the upper limb suggests that disease onset might start in a somatotopically organized fashion. Interestingly, the nigrostriatal projection does not seem to be somatotopically arranged,[45] and its dense and profuse synaptic arborization pattern is not suggestive of a highly discriminative somatotopic arrangement. On the other hand, corticostriatal projections do have a clear topographic and somatotopic distribution,[14,45] which could well provide the anatomic functional basis for the focal vulnerability.[55,56] In this regard, several not mutually exclusive mechanisms may be implicated.

First, it is worth considering that dopaminergic striatal activity normally is uneven in a dorsoventral gradient.[57,58] Accordingly, it is conceivable that the putamen subregion representing the upper limb receives a higher density of dopaminergic nigrostriatal terminals, and the hand zone in particular is more profusely innervated, in keeping with its larger homunculus representation and high movement repertoire.[18] This is in keeping with the unexpected finding in HS (Supplementary Fig. 3) whereby a net higher ^{18}F-DOPA K_i was observed in the post-commissural upper-limb division. Such an arrangement could render this zone more exposed to putative noxious agents and/or facilitate an unfavourable synapsis milieu. In other words, the formidable motor skills exhibited by the upper limbs in humans may require a degree of connectivity and dopaminergic activity that, when associated with other relevant risk factors,[59] may trigger deleterious events at nigrostriatal terminals.[60] Admittedly, this is purely hypothetical at this time.

Progression

Motor signs worsened in the upper limb and appeared in the lower limb of the MAS and upper limb of the primarily LAS over the 2-year follow-up period.[18] Thus, clinical progression followed a somatotopic pattern in keeping with previous observations.[42] In parallel, ^{18}F-DOPA PET K_i was reduced mainly in the upper limb region bilaterally, but the progression was greater in the primarily less-affected putamen. The latter, therefore, evolved to reproduce essentially the pattern found at baseline in the more-affected putamen (Fig. 2C). This evolution provides strong support to the accuracy of our findings and suggests that the same mechanism(s) operates in parallel with a time-lag of a few years (2–3 years) before reaching clinical threshold. This in turn makes it difficult to conceive that an external noxious agent (including toxic aggregation of proteins like alpha-synuclein) could impinge upon the nigrostriatal projection (neuronal SNpc soma and/or dopaminergic terminals) in an identical manner and with such a large time difference.

The pattern of reduction in ^{18}F-DOPA K_i in both hemispheres is suggestive of a radial expansion in the dorsoventral axis, with the epicentre in the upper-limb somatotopic zone and secondary involvement of adjacent dorsal and ventral areas (lower limb and face, respectively). In this regard, our study did not determine specific data for facial movements, voice and speech, which are needed to provide definitive evidence about the expansion of dopaminergic denervation and the progression of motor manifestations.

Conclusions

We describe a fairly well-defined pattern of dopaminergic nigrostriatal loss on the primarily affected side in early Parkinson's disease. A trend towards a similar pattern was found on the less-affected side after 2 years of evolution. Our findings indicate that the caudal–intermediate region of the putamen, corresponding to upper-limb somatotopic representation, is most vulnerable to neurodegeneration in both hemispheres.

Acknowledgements

We wish to thank the University Hospital HM-Puerta del Sur and in particular Dr Santiago Ruiz de Aguiar, medical director, Dr Lina Cañamaque, head of the nuclear medicine department, and the members of the Radiology Department, Silvia Casas and Ursula Alcañas, for their support. Data were provided in part by the Human Connectome Project, WU-Minn Consortium (Principal Investigators: David Van Essen and Kamil Ugurbil; 1U54MH091657) funded by the 16 NIH Institutes and Centers that support the NIH Blueprint for Neuroscience Research; and by the McDonnell Center for Systems Neuroscience at Washington University.

Funding

This work was supported by Fundación MAPFRE (Madrid, Spain), Ministerio de Ciencia e Innovación, Spanish Government (Grant number PID2019-111045RB-I00), Fundación Hospitales de Madrid (Madrid, Spain).

Competing interests

J.A.P.P. received honoraria for lecturing from GE Healthcare and Zambon. A.S.F. declares patents and stock ownership in the start-up company Leuko Labs, Inc.; received honoraria for lecturing from Abbvie, Bayer, Novartis, Parkinson's disease Monitor, Roche, SEN, Teva and Zambon and received research grants from ERA-NET Horizon 2020 program JPCOFUND2 (Reference Number: HESOCARE-329–073). N.P. received honoraria for lecturing from Britannia, Abbvie, GE Healthcare, Boston Scientific; serves in several advisory boards: Britannia, Boston Scientific, Benevolent AI, Roche, Abbvie; and received research grants from Independent Research Fund Denmark, Danish Parkinson's Disease Association, Parkinson's UK, Center of Excellence in Neurodegeneration (CoEN) network award, GE Healthcare Grant, Multiple System Atrophy Trust, Weston Brain Institute, EU Joint Program Neurodegenerative Disease Research (JPND), EU Horizon 2020 research and innovation programme and the Italian Ministry of Health. J.A.O. received honoraria for lecturing at meetings organized by GSK, Lundbeck, UCB, TEVA-Neuroscience and Boehringer Ingelheim and serves on two advisory boards (2014, 2017) on behalf of Insightec. M.H.G.M. declares no competing interests.

Supplementary material

Supplementary material is available at *Brain* online.

References

1. Fearnley JM, Lees AJ. Ageing and Parkinson's disease: Substantia nigra regional selectivity. *Brain*. 1991;114(Pt 5): 2283–2301.
2. Damier P, Hirsch EC, Agid Y, Graybiel AM. The substantia nigra of the human brain: II. Patterns of loss of dopamine-containing neurons in Parkinson's disease. *Brain*. 1999;122:1437–1448.
3. Sawle GV, Playford ED, Burn DJ, Cunningham VJ, Brooks DJ. Separating Parkinson's disease from normality. *Arch Neurol*. 1994;51(3):237–243.
4. Morrish PK, Sawle GV, Brooks DJ. Regional changes in [18F]dopa metabolism in the striatum in Parkinson's disease. *Brain*. 1996; 119(6):2097–2103.
5. Hsiao I-T, Weng Y-H, Hsieh C-J, et al. Correlation of Parkinson disease severity and ^{18}F-DTBZ positron emission tomography. *JAMA Neurol*. 2014;71(6):758–766.

6. Nandhagopal R, Kuramoto L, Schulzer M, et al. Longitudinal progression of sporadic Parkinson's disease: A multi-tracer positron emission tomography study. *Brain*. 2009;132(Pt 11): 2970–2979.
7. Morrish PK, Sawle GV, Brooks DJ. An [^{18}F]dopa-PET and clinical study of the rate of progression in Parkinson's disease. *Brain*. 1996;119(2):585–591.
8. Brück A, Aalto S, Rauhala E, Bergman J, Marttila R, Rinne JO. A follow-up study on 6-[^{18}F]Fluoro-L-dopa uptake in early Parkinson's disease shows nonlinear progressionin the putamen. *Mov Disord*. 2009;24(7):1009–1015.
9. Gallagher CL, Oakes TR, Johnson SC, et al. Rate of 6-[^{18}F]fluorodopa uptake decline in striatal subregions in Parkinson's disease. *Mov Disord*. 2011;26(4):614–620.
10. Pasquini J, Durcan R, Wiblin L, et al. Clinical implications of early caudate dysfunction in Parkinson's disease. *J Neurol Neurosurg Psychiatry*. 2019;90(10):1098–1104.
11. Pavese N, Rivero-Bosch M, Lewis SJ, Whone AL, Brooks DJ. Progression of monoaminergic dysfunction in Parkinson's disease: A longitudinal ^{18}F-dopa PET study. *Neuroimage*. 2011;56(3): 1463–1468.
12. Moore RY, Whone AL, Brooks DJ. Extrastriatal monoamine neuron function in Parkinson's disease: An ^{18}F-dopa PET study. *Neurobiol Dis*. 2008;29(3):381–390.
13. Kordower JH, Olanow CW, Dodiya HB, et al. Disease duration and the integrity of the nigrostriatal system in Parkinson's disease. *Brain*. 2013;136(Pt 8):2419–2431.
14. Takada M, Tokuno H, Nambu A, Inase M. Corticostriatal projections from the somatic motor areas of the frontal cortex in the macaque monkey: Segregation versus overlap of input zones from the primary motor cortex, the supplementary motor area, and the premotor cortex. *Exp Brain Res*. 1998;120(1):114–128.
15. Nambu A, Kaneda K, Tokuno H, Takada M. Organization of corticostriatal motor inputs in monkey putamen. *J Neurophysiol*. 2002;88(4):1830–1842.
16. Gerardin E, Lehéricy S, Pochon JB, et al. Foot, hand, face and eye representation in the human striatum. *Cereb Cortex*. 2003;13(2): 162–169.
17. Vidailhet M, Bonnet AM, Marconi R, Gouider-Khouja N, Agid Y. Do Parkinsonian symptoms and levodopa-induced dyskinesias start in the foot? *Neurology*. 1994;44(9):1613–1616.
18. Monje MHG, Sánchez-Ferro A, Pineda-Pardo JA, Vela-Desojo L, Alonso-Frech F, Obeso JA. Motor onset topography and progression in Parkinson's disease: The upper limb is first. *Mov Disord*. 2021;36(4):905–912.
19. Eidelberg D. Metabolic brain networks in neurodegenerative disorders: A functional imaging approach. *Trends Neurosci*. 2009; 32(10):548–557.
20. Van Essen DC, Smith SM, Barch DM, Behrens TEJ, Yacoub E, Ugurbil K, WU-Minn HCP Consortium. The WU-Minn Human Connectome Project: An overview. *Neuroimage*. 2013;80:62–79.
21. Giuffrida JP, Riley DE, Maddux BN, Heldmann DA. Clinically deployable Kinesia™ technology for automated tremor assessment. *Mov Disord*. 2009;24(5):723–730.
22. Paulus DH, Quick HH, Geppert C, et al. Whole-body PET/MR imaging: Quantitative evaluation of a novel model-based MR attenuation correction method including bone. *J Nucl Med*. 2015; 56(7):1061–1066.
23. Avants BB, Epstein CL, Grossman M, Gee JC. Symmetric diffeomorphic image registration with cross-correlation: Evaluating automated labeling of elderly and neurodegenerative brain. *Med Image Anal*. 2008;12(1):26–41.
24. Tustison NJ, Avants BB, Cook PA, et al. N4ITK: Improved N3 bias correction. *IEEE Trans Med Imaging*. 2010;29(6):1310–1320.
25. Coupe P, Yger P, Prima S, Hellier P, Kervrann C, Barillot C. An optimized blockwise nonlocal means denoising filter for 3-D magnetic resonance images. *IEEE Trans Med Imaging*. 2008;27(4): 425–441.
26. Smith SM. Fast robust automated brain extraction. *Hum Brain Mapp*. 2002;17(3):143–155.
27. Patenaude B, Smith SM, Kennedy DN, Jenkinson M. A Bayesian model of shape and appearance for subcortical brain segmentation. *Neuroimage*. 2011;56(3):907–922.
28. Fonov V, Evans A, McKinstry R, Almli C, Collins D. Unbiased nonlinear average age-appropriate brain templates from birth to adulthood. *Neuroimage*. 2009;47:S102-
29. Jenkinson M, Bannister P, Brady M, Smith S. Improved optimization for the robust and accurate linear registration and motion correction of brain images. *Neuroimage*. 2002;17(2):825–841.
30. Patlak CS, Blasberg RG. Graphical evaluation of blood-to-brain transfer constants from multiple-time uptake data. Generalizations. *J Cereb Blood Flow Metab*. 1985;5(4):584–590.
31. Keuken MC, Forstmann BU. Data in Brief: A probabilistic atlas of the basal ganglia using 7 T MRI. *Data Br*. 2015;4:577–582.
32. Alakurtti K, Johansson JJ, Tuokkola T, Någren K, Rinne JO. Rostrocaudal gradients of dopamine D2/3 receptor binding in striatal subregions measured with [^{11}C]raclopride and high-resolution positron emission tomography. *Neuroimage*. 2013;82: 252–259.
33. Barch DM, Burgess GC, Harms MP, et al.; WU-Minn HCP Consortium. Function in the human connectome: Task-fMRI and individual differences in behavior. *Neuroimage*. 2013;80: 169–189.
34. Glasser MF, Sotiropoulos SN, Wilson JA, et al.; WU-Minn HCP Consortium. The minimal preprocessing pipelines for the Human Connectome Project. *Neuroimage*. 2013;80:105–124.
35. Gonzalez-Escamilla G, Lange C, Teipel S, Buchert R, Grothe MJ; Alzheimer's Disease Neuroimaging Initiative. PETPVE12: An SPM toolbox for Partial Volume Effects correction in brain PET—Application to amyloid imaging with AV45-PET. *Neuroimage*. 2017;147:669–677.
36. Haber SN. The primate basal ganglia: Parallel and integrative networks. *J Chem Neuroanat*. 2003;26(4):317–330.
37. Blesa J, Pifl C, Sánchez-González MA, et al. The nigrostriatal system in the presymptomatic and symptomatic stages in the MPTP monkey model: A PET, histological and biochemical study. *Neurobiol Dis*. 2012;48(1):79–91.
38. Kish SJ, Shannak K, Hornykiewicz O. Uneven pattern of dopamine loss in the striatum of patients with idiopathic Parkinson's disease. *N Engl J Med*. 1988;318(14):876–880.
39. van der Hoorn A, Burger H, Leenders KL, de Jong BM. Handedness correlates with the dominant Parkinson side: A systematic review and meta-analysis. *Mov Disord*. 2012;27(2): 206–210.
40. Schneider SA, Drude L, Kasten M, Klein C, Hagenah J. A study of subtle motor signs in early Parkinson's disease. *Mov Disord*. 2012;27(12):1563–1566.
41. Uitti RJ, Baba Y, Wszolek ZK, Putzke DJ. Defining the Parkinson's disease phenotype: Initial symptoms and baseline characteristics in a clinical cohort. *Park Relat Disord*. 2005;11(3):139–145.
42. Poewe W, Wenning GK. The natural history of Parkinson's disease. *Ann Neurol*. 1998;44(3 Suppl 1):S1–9.
43. Pagano G, Ferrara N, Brooks DJ, Pavese N. Age at onset and Parkinson disease phenotype. *Neurology*. 2016;86(15):1400–1407.
44. Choi EY, Yeo BTT, Buckner RL. The organization of the human striatum estimated by intrinsic functional connectivity. *J Neurophysiol*. 2012;108(8):2242–2263.
45. Nambu A. Somatotopic organization of the primate basal ganglia. *Front Neuroanat*. 2011;5:26.

46. Kaasinen V, Vahlberg T. Striatal dopamine in Parkinson disease: A meta-analysis of imaging studies. *Ann Neurol*. 2017;82(6):873–882.
47. Lee CS, Samii A, Sossi V, et al. *In vivo* positron emission tomographic evidence for compensatory changes in presynaptic dopaminergic nerve terminals in Parkinson's disease. *Ann Neurol*. 2000;47(4):493–503.
48. Eshuis SA, Jager PL, Maguire RP, Jonkman S, Dierckx RA, Leenders KL. Direct comparison of FP-CIT SPECT and F-DOPA PET in patients with Parkinson's disease and healthy controls. *Eur J Nucl Med Mol Imaging*. 2009;36(3):454–462.
49. Delso G, Fürst S, Jakoby B, et al. Performance measurements of the Siemens mMR integrated whole-body PET/MR scanner. *J Nucl Med*. 2011;52(12):1914–1922.
50. Filion M, Tremblay ĹO, BéDard PJ. Effects of dopamine agonists on the spontaneous activity of globus pallidus neurons in monkeys with MPTP-induced Parkinsonism. *Brain Res*. 1991;547(1):145–149.
51. Wichmann T, Kliem MA. Neuronal activity in the primate substantia nigra pars reticulata during the performance of simple and memory-guided elbow movements. *J Neurophysiol*. 2004;91(2):815–827.
52. Rodriguez-Oroz MC, Rodriguez M, Guridi J. The subthalamic nucleus in Parkinson's disease: Somatotopic organization and physiological characteristics. *Brain*. 2001;124(9):1777–1790.
53. Theodosopoulos PV, Marks WJ, Christine C, Starr PA. Locations of movement-related cells in the human subthalamic nucleus in Parkinson's disease. *Mov Disord*. 2003;18(7):791–798.
54. Romanelli P, Esposito V, Schaal DW, Heit G. Somatotopy in the basal ganglia: Experimental and clinical evidence for segregated sensorimotor channels. *Brain Res Rev*. 2005;48(1):112–128.
55. Foffani G, Obeso JA. A cortical pathogenic theory of Parkinson's disease. *Neuron*. 2018;99(6):1116–1128.
56. Djaldetti R, Ziv I, Melamed E. The mystery of motor asymmetry in Parkinson's disease. *Lancet Neurol*. 2006;5(9):796–802.
57. Cragg SJ, Hille CJ, Greenfield SA. Dopamine release and uptake dynamics within nonhuman primate striatum *in vitro*. *J Neurosci*. 2000;20(21):8209–8217.
58. Cragg SJ, Hille CJ, Greenfield SA. Functional domains in dorsal striatum of the nonhuman primate are defined by the dynamic behavior of dopamine. *J Neurosci*. 2002;22(13):5705–5712.
59. Hernandez LF, Obeso I, Costa RM, Redgrave P, Obeso JA. Dopaminergic vulnerability in Parkinson disease: The cost of humans' habitual performance. *Trends Neurosci*. 2019;42(6):375–383.
60. Wong YC, Luk K, Purtell K, et al. Neuronal vulnerability in Parkinson disease: Should the focus be on axons and synaptic terminals? *Mov Disord*. 2019;34(10):1406–1422.